Heliyon 9 (2023) e20940

Contents lists available at ScienceDirect

Heliyon

journal homepage: www.cell.com/heliyon

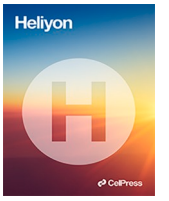

Improving near-infrared luminescence in Er^{3+} doped $CsPbBr_3$ quantum dots glasses through a certain energy transfer process

Kai Huang, Feng Jiao Zhao **, Wen Qiang Song, Chang Yuan Xu, Hong Ming Yin *

School of Science, Dalian Maritime University, Dalian, 116026, China

ARTICLE INFO

Keywords:
Er^{3+}
$CsPbBr_3$
Near infrared luminescence
Energy transfer

ABSTRACT

Er^{3+} has received extensive attention due to its excellent optical properties, especially its emission at 1535 nm in atmospheric propagation window. Enhancement and regulation of 1535 nm emission of Er^{3+} is of great significance to optical communication. In this work, growing of $CsPbBr_3$ QDs has been controlled through adjusting annealing time which would precisely regulate conduction band of $CsPbBr_3$ QDs to match energy levels of Er^{3+} enabling energy transfer between Er^{3+} and $CsPbBr_3$ QDs. By steady-state and transient PL emission and excitation spectroscopy, we reveal multiple energy transfer processes between Er^{3+} and $CsPbBr_3$ QDs under different excitation wavelengths in Er^{3+} doped $CsPbBr_3$ QDs glass: under higher energy excitation (~378 nm), energy transfer from Er^{3+} to $CsPbBr_3$ QDs and this extra energy within $CsPbBr_3$ QDs decay via a non-radiative pathway; under lower energy excitation (~524 nm), energy transfer from conduction band of $CsPbBr_3$ QDs to $^4S_{3/2}$ energy level of Er^{3+} which significantly enhances PL emission of Er^{3+} in near infrared region (~1535 nm, $^4I_{13/2} \rightarrow {}^4I_{15/2}$). These results provide a facile approach to enhance and regulate PL emission of Er^{3+} in near infrared region.

1. Introduction

In recent years, research on rare earth ions doped cesium lead halide perovskite ($CsPbX_3$, X = Cl, Br, I) quantum dots (QDs) has extensively increased due to the rich energy level structure of rare earth ions which yields unique optical properties and exceptional optical characteristics of $CsPbX_3$ [1–5]. $CsPbX_3$ has been widely used in the field of optoelectronics in the last decade, such as light-emitting diodes (LEDs), lasers, soler cell, photodetection and gamut displays [6–13]. From previous studies, photoluminescence (PL) emission of $CsPbX_3$ QDs can be tuned by adjusting size of QDs or composition of halide and accompanied with high photoluminescence quantum yields (PLQY). However, PL emission wavelength of $CsPbX_3$ QDs is commonly below 1000 nm with bandgap ranges between 1.7 and 3.1 eV [14–18]. According to the prediction for stability of perovskites, Goldschmidt tolerance factor (t) and octahedral factor (μ) of an ideal 3D perovskite structure follow expression:

$$t = \frac{r_{A+}r_X}{\sqrt{2}(r_B + r_X)} \tag{1}$$

* Corresponding author.
** Corresponding author.
E-mail addresses: fzhao@dlmu.edu.cn (F.J. Zhao), hmyin@dlmu.edu.cn (H.M. Yin).

https://doi.org/10.1016/j.heliyon.2023.e20940
Received 15 May 2023; Received in revised form 5 October 2023; Accepted 11 October 2023
Available online 13 October 2023

$$\mu = \frac{r_B}{r_X} \tag{2}$$

here in equations (1) and (2), r_B, r_X and r_X represents the radius of monovalent cation, divalent metal cation and monovalent halide anion of perovskite (ABX_3) QDs, respectively. Typically, t and μ are within 0.76–1.13 and 0.44–0.9, respectively (eg: $CsPbI_3$: $t \sim 0.8$, $\mu \sim 0.54$; $CsPbBr_3$: $t \sim 0.81$, $\mu \sim 0.61$) [6,19,20]. Due to structural flexibility of halide perovskites, heterogeneous ions can be introduced to halide perovskite [2,21,22]. Fortunately, based on luminescence properties of rare earth ions 4f electrons transitioning between different energy levels, doping of rare earth ions into $CsPbX_3$ QDs can greatly expand their PL emission range [1,23,24]. Er^{3+}, has excellent optical properties due to its abundant energy levels and relatively more discrete energy levels which reduces the occurrence of non-radiative transitions [25,26]. Generally, the most researched on Er^{3+} is its up-conversion luminescence, that is, conversion of low-energy photon into high-energy photon [27]. Especially, among many transitions between intermediate energy levels of Er^{3+}, the strong near infrared (NIR) emission at about 1535 nm ($^4I_{13/2} \rightarrow {}^4I_{15/2}$) has attracted great attention because 1535 nm is located in atmospheric window and is of great significance for long distance action [28–30]. If emission intensity of Er^{3+} at 1535 nm is further improved, it will have great potentials and actual values for applications in field of optical communications.

In previous works, energy transfer between Er^{3+} and $CsPbX_3$ QDs are commonly achieved by means of co-doping which another rare earth ion or metal ion is needed as an "intermediate bridge". Artizzu et al. achieved emission of Er^{3+} at ~1500 nm with long lifetime (~3 ms) by co-doping of Er^{3+} and Yb^{3+} in $CsPbCl_3$ nanocrystals since $^4I_{11/2}$ energy level of Er^{3+} and $^2F_{5/2}$ energy level of Yb^{3+} are resonant, and they further achieved a strong emission of Er^{3+} at 1542 nm by co-doping of Mn^{2+} and Er^{3+} in $CsPbCl_3$ nanocrystals [17,31]. Considering that the interactions like direct energy conversion process between $CsPbX_3$ QDs and Er^{3+} would greatly affect PL emission at ~1500 nm, underlying mechanism need to be further explored.

According to the resonance energy transfer theory, luminescence enhancement at 1535 nm can also be achieved by regulating energy level position and single doping Er^{3+} in $CsPbBr_3$ QDs. Therefore, in this paper, single rare ion of Er^{3+} doped $CsPbBr_3$ QDs tellurate glasses has been successfully synthesized and enhanced PL emission at 1535 nm has been achieved. By steady-state and transient spectroscopy, multiple energy transfer processes between Er^{3+} and $CsPbBr_3$ QDs have been observed. Furthermore, spectra results reveal that annealing treatment dramatically change energy levels of $CsPbBr_3$ QDs which allows energy transfer from conduction band (CB) of $CsPbBr_3$ QDs to $^4S_{3/2}$ energy level of Er^{3+} under 524 nm excitation and finally increases the PL emission at 1535 nm.

2. Materials and methods

All samples were made following traditional high-temperature melting and heat treatment method based on previous studies, which is commonly used to prepare QDs [32,33]. TeO_2 (99.99 %, Aladdin), Al_2O_3 (99.999 %, Aladdin), H_3BO_3 (99.99 %, Aladdin), ZnO (99.99 %, Aladdin), Na_2CO_3 (99.99 %, Aladdin), CaF_2 (Analytically pure, Tianjin Zhiyuan Chemical), ErF_3 (99.9 %, Aladdin), CsBr (99.999 %, Aladdin) and $PbBr_2$ (99 %, Aladdin) were used as purchased without further purification.

Proportion and molar ratio of Er^{3+} doped $CsPbBr_3$ QDs: $77TeO_2$-$1.5Al_2O_3$–$21H_3BO_3$–$18ZnO$–$14Na_2CO_3$-$9.6CaF_2$-$2.2ErF_3$–$7CsBr$-$7.1PbBr_2$. In contrast, non-doping $CsPbBr_3$ QDs samples share the same synthesis proportioning as above but do not contain ErF_3. For all ingredients, total mass of 5 g for all samples were weighed. Powder were mixed in an agate mortar and grinded for 20 min, then the mixture were moved to a crucible and melt at 850 °C for 30 min. The melted samples were cooled at room temperature and molded to form the precursor glass sheet with 2 mm thickness. After calcification at 260 °C for 180 min, a portion was annealed at 320 °C for 90 min and 180 min, respectively.

Transmission electron microscopy (TEM) images of $CsPbBr_3$ QDs tellurate glasses after 90 min annealing treatment at 320 °C was obtained with ultra-high resolution transmission electron microscope. Accelerating voltage was 200 KV and magnification was 800,000 times. For TEM measurement, solvent used during sample preparation process was anhydrous ethanol. Then $CsPbBr_3$ QDs

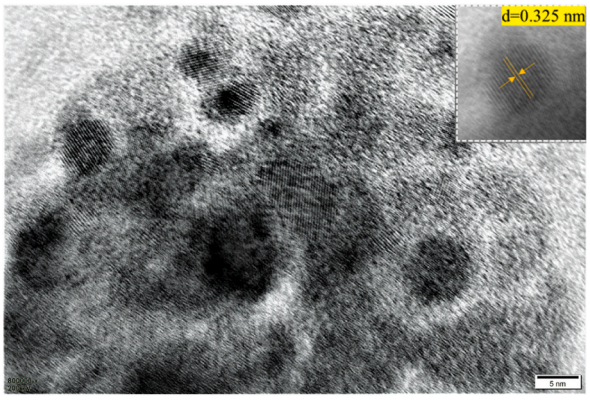

Fig. 1. Transmission electron microscopy (TEM) image of $CsPbBr_3$ QDs after 90 min annealing treatment at 320 °C (the inset shows the lattice spacing).

glass was ground, dissolved, oscillated by ultrasonic, dropped to the microgrid, and dried to obtain TEM test sample.

Transient emission (TE) spectra and decay dynamics curves were obtained using self-built high spatial resolution laser-induced nanosecond transient spectra acquisition system with emission wavelength ranging from 460 nm to 580 nm [34,35]. Nd: YAG laser provides 532 nm output which was introduced into a dye laser equipped with dye of LD 700 which yields laser output from 355 nm to 385 nm. Through setting of self-built high spatial resolution laser-induced nanosecond transient spectra acquisition system by control unit, output frequency of dye laser was 3 Hz and output energy was 200 μW (measured by an energy meter, LabMax TOP, Coherent Co.). Excitation spectra and steady state emission spectra were collected using steady state/transient fluorescence spectrometer FLS1000 (Edinburgh Instruments). It has to be noted that, in order to maintain the original optical properties of all samples and make them comparable, all glass samples share the same thickness and no extra processing have been done like polishing.

3. Results and discussion

In order to reveal the crystallization and size of $CsPbBr_3$ QDs, TEM image of $CsPbBr_3$ QDs tellurate glass after 90 min annealing treatment at 320 °C was measured. From Fig. 1, it can be found that $CsPbBr_3$ QDs present a spherical shape with diameter ranging from 5 nm to 10 nm. Inset in Fig. 1 shows lattice spacing of d = 0.325 nm which corresponds to (111) lattice plane of $CsPbBr_3$ QDs. From TEM results, $CsPbBr_3$ QDs were successfully grown with obvious lattice structure in tellurate glass substrate after high temperature melting and low temperature annealing treatment.

To better understand PL emission properties of Er^{3+} doped $CsPbBr_3$ QDs, TE spectra of all samples are measured under 377.5 nm excitation and results are shown in Fig. 2. Fig. 2 shows the transient emission spectrum of samples, where the horizontal coordinate is wavelength and the vertical coordinate is time, representing the relationship between the luminous intensity and time, in which different mapped colors represent the luminous lifetime at different moments. From Fig. 2(a), non-doped $CsPbBr_3$ QDs with annealing time of 90 min show PL emission from 460 nm to 560 nm which centered at 504 nm. With longer annealing time of 180 min, as shown in Fig. 2(b), PL emission in this range has been enhanced and presents redshift from 504 nm to 514 nm. This can be explained that $CsPbBr_3$ QDs crystallize and grow during annealing process and longer annealing time would yield more $CsPbBr_3$ QDs with larger size which corresponds to enhancement and redshift of PL emission, respectively [36–38]. Herein, PL emission properties of $CsPbBr_3$ QDs can be easily tuned by adjusting annealing time. Comparing with non-doped $CsPbBr_3$ QDs, Er^{3+} doped $CsPbBr_3$ QDs (Fig. 2c-d) show weaker PL emission during 460 nm–560 nm range which suggests that interactions between Er^{3+} and $CsPbBr_3$ QDs would weaken PL emission. Also, with annealing time has been prolonged, PL emission peak gets decreased which further indicates growing of $CsPbBr_3$ QDs improves such interaction between Er^{3+} and $CsPbBr_3$ QDs. Moreover, PL emission redshift from 504 nm to 514 nm also occurs for Er^{3+} doped $CsPbBr_3$ QDs. It has to be noted that, from Fig. 2, PL emission was markedly weakened with wavelength ≥524 nm of Er^{3+} doped $CsPbBr_3$ QDs compared with undoped $CsPbBr_3$ QDs. Especially, for Er^{3+} doped $CsPbBr_3$ QDs, the characteristic PL emission of Er^{3+} at 556 nm gets weaker with longer annealing time. Therefore, from TE spectra, population of electrons locate at lower energy levels (≥524 nm) has been reduced result from Er^{3+} doping.

To figure out mechanism of Er^{3+} affecting PL emission of $CsPbBr_3$ QDs, PL decay kinetics curves at both 510 nm and 524 nm are fitted and results are shown in Fig. 3 and Table 1. In order to show the PL decay kinetics curves more intuitively, intensity of PL decay kinetics curves was normalized and displayed in a logarithmic scale. Biexponential function was used to fit these decay kinetics curves with expression written as

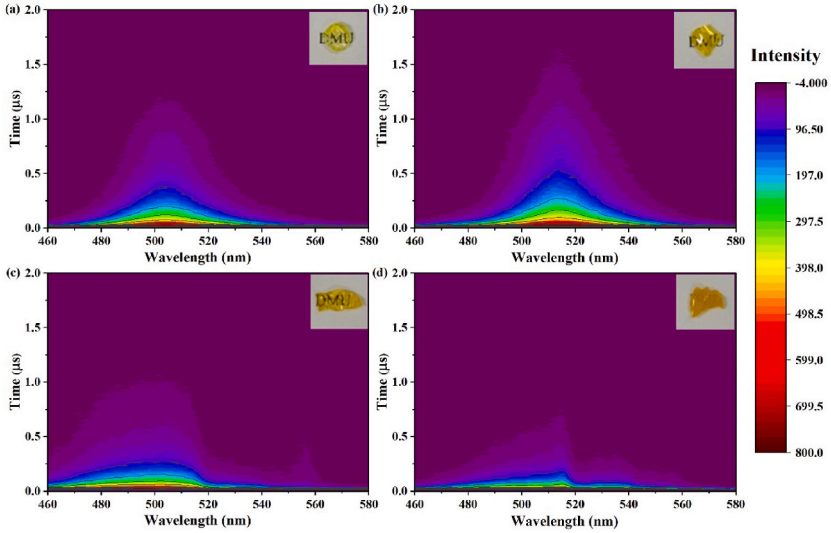

Fig. 2. Transient emission (TE) spectra of non-doped $CsPbBr_3$ QDs after 90 min **(a)** and 180 min **(b)** annealing treatment at 320 °C and Er^{3+} doped $CsPbBr_3$ QDs after 90 min **(c)** and 180 min **(d)** annealing treatment at 320 °C excited at 377.5 nm (the insets are photos of samples).

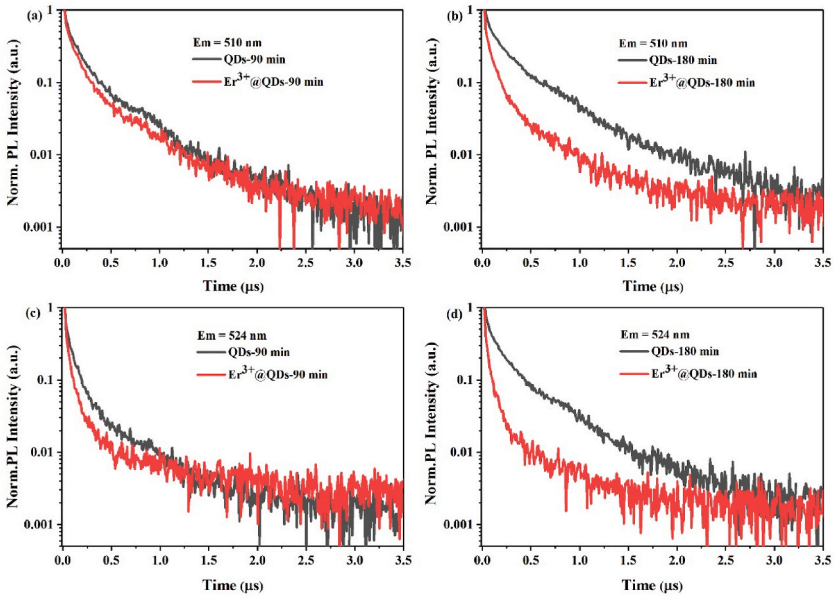

Fig. 3. PL decay kinetics curves of $CsPbBr_3$ QDs and Er^{3+} doped $CsPbBr_3$ QDs after 90 min **(a)** and 180 min **(b)** annealing treatment at 510 nm emission and $CsPbBr_3$ QDs and Er^{3+} doped $CsPbBr_3$ QDs after 90 min **(c)** and 180 min **(d)** annealing treatment at 524 nm emission. Excitation wavelength was set as 377.5 nm.

Table 1
Fitting parameters of decay kinetics curves of $CsPbBr_3$ QDs and Er^{3+} doped $CsPbBr_3$ QDs in Fig. 3.

			τ_1 (μs)	A_1	τ_2 (μs)	A_2	Adj.R-Square
510 nm	90min	QDs	0.046	0.978	0.291	0.407	0.996
		Er^{3+}@QDs	0.031	1.132	0.213	0.434	0.996
	180min	QDs	0.061	0.856	0.411	0.435	0.998
		Er^{3+}@QDs	0.018	1.951	0.143	0.405	0.995
524 nm	90min	QDs	0.019	1.762	0.134	0.446	0.995
		Er^{3+}@QDs	0.014	3.102	0.086	0.363	0.997
	180min	QDs	0.046	0.990	0.333	0.391	0.997
		Er^{3+}@QDs	0.012	3.894	0.082	0.365	0.997

Note: τ is lifetime, A is corresponding amplitude.

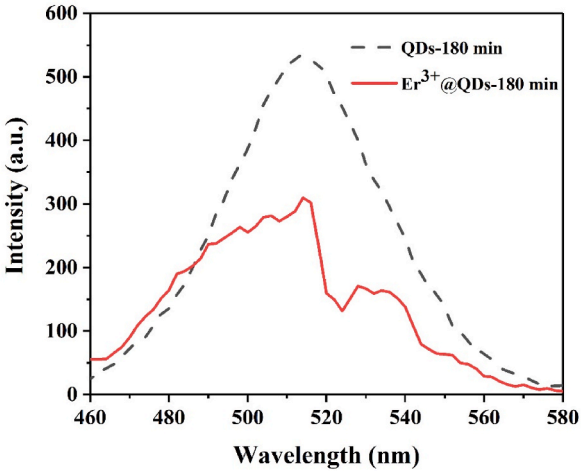

Fig. 4. Transient PL emission spectra at 0.06 us of $CsPbBr_3$ QDs and Er^{3+} doped $CsPbBr_3$ QDs with annealing time of 180 min under 377.5 nm excitation.

$$I = A_1 * exp(-k / \tau_1) + A_2 * exp(-k / \tau_2) + I_0 \quad (3)$$

From Fig. 3 (a) and 3 (c), under excitation of 377.5 nm, for both Er^{3+} doped and undoped $CsPbBr_3$ QDs with 90 min annealing process, PL emission at both 510 nm and 524 nm present similar decay trend.

However, when annealing time was increased to 180 min, as shown in Fig. 3 (b) and (d), Er^{3+} doped $CsPbBr_3$ QDs show markedly faster decay processes at both 510 nm and 524 nm compared with undoped $CsPbBr_3$ QDs, respectively. Lifetime of all samples are listed in Table 1. This can be explained as redshift of PL emission induced by increase of annealing time which promotes doping of Er^{3+} into $CsPbBr_3$ QDs and might enable efficient energy transfer from $CsPbBr_3$ QDs to Er^{3+}. Especially, for $CsPbBr_3$ QDs, as redshift of PL emission peak from 504 nm to 514 nm, CB of $CsPbBr_3$ QDs gets closer to $^2H_{11/2}$ energy level of Er^{3+}, which further facilitates efficient energy transfer process to occur from $CsPbBr_3$ QDs to Er^{3+}.

To verify energy transfer process, transient PL emission spectra ranging from 460 nm to 580 nm of $CsPbBr_3$ QDs and Er^{3+} doped $CsPbBr_3$ QDs with annealing time of 180 min are compared and displayed in Fig. 4. From values of τ_2 for these two samples, transient PL emission spectra before 0.082 μs could reveal PL emission character before decay process and thus, PL emission spectra at 0.06 μs was presented. It can be found that, under excitation of 377.5 nm, doping of Er^{3+} significantly reduces PL emission of $CsPbBr_3$ QDs at range of 480 nm–540 nm. In order to quantitatively compare the luminous intensity of $CsPbBr_3$ QDs and Er^{3+} doped $CsPbBr_3$ QDs, we calculated the integral values in the range of 480 nm–540 nm as shown in Fig. 4, and the results were 22394 and 13047, respectively, which yield the ratio of 1.72. The values 22394 and 13047 can be understood as the number of photons emitted by $CsPbBr_3$ QDs and Er^{3+} doped $CsPbBr_3$ QDs when the excitation light intensity is the same. Therefore, PL emission of $CsPbBr_3$ QDs during this range has been reduced by 41.74 % via doping of Er^{3+}.

To figure out specific decay pathway of such 41.74 % PL emission loss, PL excitation spectra (emission monitored at 1535 nm) of Er^{3+} doped $CsPbBr_3$ QDs with different time of annealing treatment (0 min, 90 min and 180 min) in 200–600 nm range have been measured and shown in Fig. 5. Due to the influence of matrix-related stresses on QDs, raw glass samples of the same thickness without any further processing were used in measurements of steady-state PL excitation spectra and PL emission spectra of Er^{3+} doped $CsPbBr_3$ QDs with 0 min, 90 min and 180 min annealing treatment at 320 °C [39]. From Fig. 5(A), for Er^{3+} doped $CsPbBr_3$ QDs without annealing process which is precursor, dense PL excitation peaks appear in the range of 200 nm–600 nm locating at 366 nm, 378 nm, 407 nm, 443 nm, 451 nm, 488 nm, 521 nm and 544 nm which correspond to Er^{3+} energy levels of $^2G_{9/2}$, $^4G_{11/2}$, $^2H_{9/2}$, $^4F_{3/2}$, $^4F_{5/2}$, $^4F_{7/2}$, $^2H_{11/2}$ and $^4S_{3/2}$, respectively.

In contrast, after 90 min annealing treatment, in Fig. 5(B), PL excitation peaks in 200 nm–600 nm range are reduced to four peaks which locate at 378 nm, 488 nm, 521 nm and 544 nm. Furthermore, with longer annealing time of 180 min (Fig. 5(C)), only three PL excitation peaks remain at 378 nm, 524 nm and 544 nm. It has to be noted that main PL excitation peaks of Er^{3+} doped $CsPbBr_3$ precursor appear at 378 nm ($^4G_{11/2}$) and 521 nm ($^2H_{11/2}$), and dominate PL excitation peaks of Er^{3+} doped $CsPbBr_3$ QDs annealed for 90 min and 180 min are at 521 nm ($^2H_{11/2}$) and 524 nm ($^2H_{11/2}$), respectively. These PL excitation spectra results indicate that $CsPbBr_3$ QDs have strong interactions with doped Er^{3+} which eliminate high PL excitation energy levels which could emit PL at 1535 nm.

To further investigate PL emission loss and interactions between Er^{3+} and $CsPbBr_3$ QDs which affect PL excitation energy levels of Er^{3+}, measurement of PL emission spectra ranging from 1400 nm to 1700 nm which aims at characteristic PL emission peak of Er^{3+} of Er^{3+} doped $CsPbBr_3$ precursor and Er^{3+} doped $CsPbBr_3$ QDs with 180 min annealing treatment under excitation of 378 nm and 524 nm have been conducted and results are shown in Fig. 6. From PL excitation spectra, 378 nm and 524 nm correspond to Er^{3+} energy levels of $^4G_{11/2}$ and $^2H_{11/2}$ which generate PL emission at 1535 nm, thus, PL emission spectra under both 378 nm and 524 nm could provide comparation of interactions between relatively high/low excitation energy levels of Er^{3+} and $CsPbBr_3$ QDs. To better compare PL emission of all samples under different excitation wavelengths, PL emission spectra in Fig. 6 have been modified with the same PL excitation intensity. It can be found that, from Fig. 6 (a), under 378 nm excitation, PL emission of Er^{3+} doped $CsPbBr_3$ QDs at 1535 nm

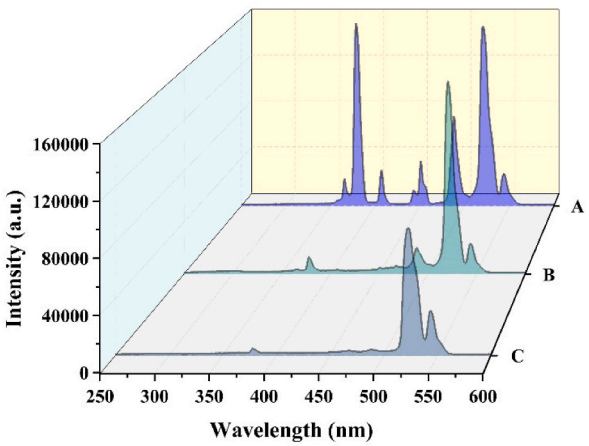

Fig. 5. PL Excitation spectra of Er^{3+} doped $CsPbBr_3$ QDs with annealing time of 0 min **(A)**, 90 min **(B)** and 180 min **(C)**. PL emission is monitored at 1535 nm.

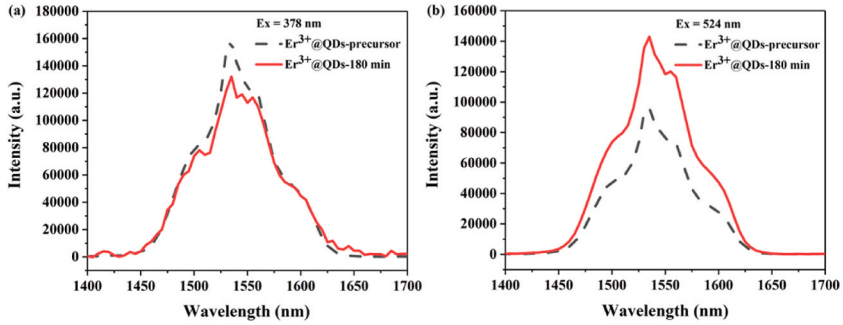

Fig. 6. The modified PL emission spectra of Er^{3+} doped $CsPbBr_3$ QDs precursor and after annealing for 180 min under 378 nm **(a)** and 524 nm **(b)** excitation, respectively.

after annealing for 180 min is slightly weaker than that of Er^{3+} doped $CsPbBr_3$ QDs precursor without annealing. However, from Fig. 6 (b), Er^{3+} doped $CsPbBr_3$ QDs after annealing for 180 min has much stronger PL emission at 1535 nm compare with Er^{3+} doped $CsPbBr_3$ QDs precursor under 524 nm excitation. This result reveals that interactions between CB of $CsPbBr_3$ QDs and $^4G_{11/2}/^2H_{11/2}$ energy levels of Er^{3+} represent different mechanism and excitation of lower energy level (bandgap @524 nm) would facilitate energy transfer process from $CsPbBr_3$ QDs to Er^{3+} which leads to stronger emission at 1535 nm of Er^{3+}. To quantitatively compare PL emission character, integration of PL emission peaks centered at 1535 nm in Fig. 6 have also been calculated from 1400 nm to 1700 nm. For 378 nm excitation in Fig. 6 (a), peak area integrations are 11618662 and 12454580 for Er^{3+} doped $CsPbBr_3$ QDs with and without annealing treatment, respectively. In this case, PL emission intensity ratio is 0.93. For 524 nm excitation in Fig. 6 (b), peak area integrations are 11947450 and 7545520 for Er^{3+} doped $CsPbBr_3$ QDs with and without annealing treatment which yield the ratio of 1.58. Obviously, ratio of 1.58 in Fig. 6 (b) corresponds to ratio 1.72 in Fig. 4 which further supports mechanism of energy transfer process from $CsPbBr_3$ QDs to Er^{3+} in sample of Er^{3+} doped $CsPbBr_3$ QDs after 180 min of annealing.

Based on spectral results above, the specific energy transfer processes between $CsPbBr_3$ QDs and Er^{3+} can be illustrated in diagram (Fig. 7). For PL excitation spectra (monitored@1535 nm), when PL excitation wavelength is below 500 nm, six PL excitation peaks (@366 nm, 378 nm, 407 nm, 443 nm, 451 nm and 488 nm) of Er^{3+} doped $CsPbBr_3$ precursor show up. However, when annealing time increases, number of PL excitation peaks gets significantly reduced to two (@378 nm and 488 nm) and one (@378 nm) for 90 min and 180 min annealing treatment, respectively. Moreover, under 378 nm excitation, Er^{3+} doped $CsPbBr_3$ QDs with 180 min annealing treatment shows weaker PL emission at 1535 nm comparing with that of unannealed Er^{3+} doped $CsPbBr_3$ precursor. Therefore, generation of $CsPbBr_3$ QDs gradually weaken PL excitation at high energy levels of Er^{3+} which indicates energy transfer from Er^{3+} to $CsPbBr_3$ QDs under high energy excitation. Meanwhile, from Fig. 2 (c)–(d), PL emission of $CsPbBr_3$ QDs has not been enhanced after energy transfer from Er^{3+} to $CsPbBr_3$ QDs under 377.5 nm excitation, thus, energy transferred to $CsPbBr_3$ QDs does not annihilate via photon emission. Also, from Fig. 6 (a), PL emission at 1535 nm of Er^{3+} does not either enhanced under 378 nm excitation which suggests that $CsPbBr_3$ QDs does not either transfer energy back to Er^{3+}. As a result, under high energy excitation, energy transferred from Er^{3+} to $CsPbBr_3$ QDs annihilate via a non-irradiative pathway. This explanation is supported by previous spectral results: infrared PL emission of Er^{3+} ($^4I_{13/2} \rightarrow {}^4I_{15/2}$) cannot be seen in Er^{3+} doped $CsPbCl_3$ QDs under 365 nm excitation, but it showed up when Er^{3+} and Yb^{3+} were co-doped into $CsPbCl_3$ QDs [40]; Zhang et al. found that when Er^{3+} has been doped $CsPbCl_3$ nanocrystals, PL emission of Er^{3+} in near infrared cannot be observed experimentally [41]. When PL excitation wavelength is larger than 500 nm, from Fig. 6 (b), excitation at 524 nm which corresponds to $^2H_{11/2}$ energy level of Er^{3+} markedly enhanced PL emission of Er^{3+} in near infrared with 180 min annealing treatment of $CsPbBr_3$ QDs. Commonly, under 524 nm excitation, excited electrons at $^2H_{11/2}$ energy level of Er^{3+} decay back to ground state of $^4I_{15/2}$ through $^4S_{3/2}$, $^4F_{9/2}$, $^4I_{9/2}$, $^4I_{11/2}$ and $^4I_{13/2}$, and final transition from $^4I_{13/2}$ to $^4I_{15/2}$ yields 1535 nm PL emission. In this work, with growing of $CsPbBr_3$ QDs, CB of $CsPbBr_3$ QDs gradually approaches $^2H_{11/2}$ energy level of Er^{3+} which makes it possible for $CsPbBr_3$ QDs to transfer energy from CB of $CsPbBr_3$ QDs to $^4S_{3/2}$ of Er^{3+}. Then, excited $^4S_{3/2}$ energy level of Er^{3+} goes through normal decay process which finally enhance the 1535 nm emission.

4. Conclusions

In summary, growing of $CsPbBr_3$ QDs can be controlled through adjusting annealing time which would regulate CB of $CsPbBr_3$ QDs to match energy levels of Er^{3+}. By steady-state and transient PL emission and excitation spectra combining with decay kinetics fittings, we found multiple energy transfer processes between Er^{3+} and $CsPbBr_3$ QDs under different excitation wavelengths in Er^{3+} doped $CsPbBr_3$ QDs glass: under higher energy excitation (~378 nm), energy transfer from Er^{3+} to $CsPbBr_3$ QDs and this extra energy within $CsPbBr_3$ QDs decay via a non-radiative pathway; under lower energy excitation (~524 nm), energy transfer from CB of $CsPbBr_3$ QDs to $^4S_{3/2}$ energy level of Er^{3+} which significantly enhances PL emission of Er^{3+} in near infrared region (~1535 nm, $^4I_{13/2} \rightarrow {}^4I_{15/2}$). These results provide a facile approach to regulate energy levels of $CsPbBr_3$ QDs to further enhance near-infrared emission of Er^{3+}.

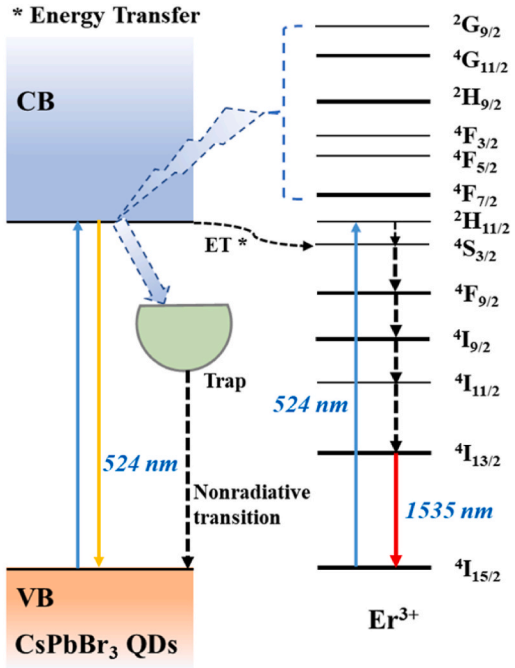

Fig. 7. Schematic illustration of energy transfer processes between Er^{3+} and $CsPbBr_3$ QDs of Er^{3+} doped $CsPbBr_3$ QDs after 180 min of annealing at 320 °C.

Data availability statement

Data associated with this study has not been deposited into a publicly available repository. Data will be made available on request.

CRediT authorship contribution statement

Kai Huang: Data curation, Formal analysis. **Feng Jiao Zhao:** Formal analysis, Funding acquisition, Investigation, Supervision, Writing – original draft, Writing – review & editing. **Wen Qiang Song:** Data curation, Methodology. **Chang Yuan Xu:** Data curation, Methodology. **Hong Ming Yin:** Conceptualization, Formal analysis, Investigation, Methodology, Project administration, Supervision, Writing – review & editing.

Declaration of competing interest

The authors declare that they have no known competing financial interests or personal relationships that could have appeared to influence the work reported in this paper.

Acknowledgement

The authors gratefully acknowledge the financial support from the Fundamental Research Funds for the Central Universities (Grant No. 3132023197).

References

[1] G.C. Pan, X. Bai, D.W. Yang, X. Chen, P.T. Jing, S.N. Qu, L.J. Zhang, D.L. Zhou, J.Y. Zhu, W. Xu, B. Dong, H.W. Song, Doping lanthanide into perovskite nanocrystals: highly improved and expanded optical properties, Nano Lett. 17 (2017) 8005–8011.
[2] D.L. Zhou, D.L. Liu, G.C. Pan, X. Chen, D.Y. Li, W. Xu, X. Bai, H.W. Song, Cerium and Ytterbium codoped halide perovskite quantum dots: a novel and efficient downconverter for improving the performance of silicon solar cells, Adv. Mater. 29 (2017), 1704149.
[3] W.J. Mir, Y. Mahor, A. Lohar, M. Jagadeeswararao, S. Das, S. Mahamuni, A. Nag, Postsynthesis doping of Mn and Yb into $CsPbX_3$ (X = Cl, Br, or I) perovskite nanocrystals for downconversion emission, Chem. Mater. 30 (2018) 8170–8178.
[4] Y. Mahor, W.J. Mir, A. Nag, Synthesis and near-infrared emission of Yb-doped $Cs_2AgInCl_6$ double perovskite microcrystals and nanocrystals, J. Phys. Chem. C 123 (2019) 15787–15793.
[5] L.J. He, J.L. Meng, J. Feng, X.J. Liu, H.J. Zhang, Unveiling the mechanism of rare earth doping to optimize the optical performance of the $CsPbBr_3$ perovskite, Inorg. Chem. Front. 7 (2020) 4669–4676.
[6] J. Shamsi, A.S. Urban, M. Imran, L. De Trizio, L. Manna, Metal halide perovskite nanocrystals: synthesis, post-synthesis modifications, and their optical properties, Chem. Rev. 119 (2019) 3296–3348.

[7] J.L. Duan, Y.Y. Zhao, Y.D. Wang, X.Y. Yang, Q.W. Tang, Hole-boosted Cu(Cr, M)O_2 nanocrystals for all-inorganic $CsPbBr_3$ perovskite solar cells, Angew. Chem. Int. Ed. 58 (2019) 16147–16151.
[8] Y. Wang, L. Song, Y. Chen, W. Huang, Emerging new-generation photodetectors based on low-dimensional halide perovskites, ACS Photonics 7 (2020) 10–28.
[9] X.X. Wang, H.Z. Chen, H. Zhou, X. Wang, S.P. Yuan, Z.Q. Yang, X.L. Zhu, R.M. Ma, A.L. Pan, Room-temperature high-performance $CsPbBr_3$ perovskite tetrahedral microlasers, Nanoscale 11 (2019) 2393–2400.
[10] Q.A. Akkerman, V. D'Innocenzo, S. Accornero, A. Scarpellini, A. Petrozza, M. Prato, L. Manna, Tuning the optical properties of Cesium Lead halide perovskite nanocrystals by anion exchange reactions, J. Am. Chem. Soc. 137 (2015) 10276–10281.
[11] Y.X. Li, X.Y. Zhang, H. Huang, S.V. Kershaw, A.L. Rogach, Advances in metal halide perovskite nanocrystals: synthetic strategies, growth mechanisms, and optoelectronic applications, Mater. Today Off. 32 (2020) 204–221.
[12] Y. Kanemitsu, Halide perovskite nanocrystals: unique luminescence materials, J. Lumin. 251 (2022), 119207.
[13] Y. Xu, S.Q. Lou, C. Xia, T.T. Xuan, H.L. Li, Controllable synthesis of all inorganic lead halide perovskite nanocrystals and white light-emitting diodes based on $CsPbBr_3$ nanocrystals, J. Lumin. 222 (2020), 117132.
[14] L. Protesescu, S. Yakunin, M.I. Bodnarchuk, F. Krieg, R. Caputo, C.H. Hendon, R.X. Yang, A. Walsh, M.V. Kovalenko, Nanocrystals of Cesium Lead halide perovskites ($CsPbX_3$, X= Cl, Br, and I): novel optoelectronic materials showing bright emission with wide color gamut, Nano Lett. 15 (2015) 3692–3696.
[15] Y.L. Li, X. Luo, T. Ding, X. Lu, K.F. Wu, Size and halide dependent auger recombination in Lead halide perovskite nanocrystals, Angew. Chem., Int. Ed. 59 (2020) 14292–14295.
[16] M. Imran, V. Caligiuri, M.J. Wang, L. Goldoni, M. Prato, R. Krahne, L. De Trizio, L. Manna, Benzoyl halides as alternative precursors for the colloidal synthesis of Lead-based halide perovskite nanocrystals, J. Am. Chem. Soc. 140 (2018) 2656–2664.
[17] M. Zeng, F. Locardi, D. Mara, Z. Hens, R. Van Deun, F. Artizzu, Switching on near-infrared light in lanthanide-doped $CsPbCl_3$ perovskite nanocrystals, Nanoscale 13 (2021) 8118–8125.
[18] F.J. Zeng, Y.Y. Guo, W. Hu, Y.Q. Tan, X.M. Zhang, J. Yang, Q.Q. Lin, Y. Peng, X.S. Tang, Z.Z. Liu, Z.Q. Yao, J. Du, Green anti-solvent assisted crystallization strategy for air-stable uniform $Cs_3Cu_2I_5$ perovskite films with highly efficient blue photoluminescence, J. Lumin. 223 (2020), 117178.
[19] J.S. Manser, J.A. Christians, P.V. Kamat, Intriguing optoelectronic properties of metal halide perovskites, Chem. Rev. 116 (2016) 12956–13008.
[20] C.H. Li, X.G. Lu, W.Z. Ding, L.M. Feng, Y.H. Gao, Z.G. Guo, Formability of ABX_3 (X = F, Cl, Br, I) halide perovskites, Acta Crystallogr. Sect. B 64 (2008) 702–707.
[21] Y.H. Chen, S.C. Liu, N. Zhou, N.X. Li, H.P. Zhou, L.D. Sun, C.H. Yan, An overview of rare earth coupled lead halide perovskite and its application in photovoltaics and light emitting devices, Prog. Mater. Sci. 120 (2020), 100737.
[22] W.C. Xiang, Z.W. Wang, D.J. Kubicki, W. Tress, J.S. Luo, D. Prochowicz, S. Akin, L. Emsley, J.T. Zhou, G. Dietler, M. Gratzel, A. Hagfeldt, Europium-doped $CsPbI_2Br$ for stable and highly efficient inorganic perovskite solar cells, Joule 3 (2019) 205–214.
[23] P.J.S. Rana, T. Swetha, H. Mandal, A. Saeki, P.R. Bangal, S.P. Singh, Energy transfer dynamics of highly stable Fe^{3+} doped $CsPbCl_3$ perovskite nanocrystals with dual-color emission, J. Phys. Chem. C 123 (2019) 17026–17034.
[24] M. Righetto, D. Meggiolaro, A. Rizzo, R. Sorrentino, Z.B. He, G. Meneghesso, T.C. Sum, T. Gatti, F. Lamberti, Coupling halide perovskites with different materials: from doping to nanocomposites, beyond photovoltaics, Prog. Mater. Sci. 110 (2020), 100639.
[25] H. Dong, L.D. Sun, C.H. Yan, Basic understanding of the lanthanide related upconversion emissions, Nanoscale 5 (2013) 5703–5714.
[26] B. Zhou, B.Y. Shi, D.Y. Jin, X.G. Liu, Controlling upconversion nanocrystals for emerging applications, Nat. Nanotechnol. 10 (2015) 924–936.
[27] H. Dong, L.D. Sun, C.H. Yan, Energy transfer in lanthanide upconversion studies for extended optical applications, Chem. Soc. Rev. 44 (2015) 1608–1634.
[28] H.Q. Ye, Z. Li, Y. Peng, C.C. Wang, T.Y. Li, Y.X. Zheng, A. Sapelkin, G. Adamopoulos, I. Hernandez, P.B. Wyatt, W.P. Gillin, Organo-Erbium systems for optical amplification at telecommunications wavelengths, Nat. Mater. 13 (2014) 382–386.
[29] T. Koonen, K. Mekonnen, Z.Z. Cao, F. Huijskens, N.Q. Pham, E. Tangdiongga, Ultra-high-capacity wireless communication by means of steered narrow optical beams, Philos. T. R. SOC. A. 378 (2020), 20190192.
[30] Z. Leng, X. Zhang, X.M. Shi, W.L. Yang, C. Li, X.L. Jiang, D.M. Wang, F.M. Zeng, C. Li, H. Lin, Z.M. Su, Near-infrared luminescence of Er^{3+} doped $Na_{0.04}K_{0.96}Y(WO_4)_2$ single crystals, J. Lumin. 250 (2022), 119030.
[31] M. Zeng, F. Artizzu, J. Liu, S. Singh, F. Locardi, D. Mara, Z. Hens, R. Van Deun, Boosting the Er^{3+} 1.5 μm luminescence in $CsPbCl_3$ perovskite nanocrystals for photonic devices operating at telecommunication wavelengths, ACS Appl. Nano Mater. 3 (2020) 4699–4707.
[32] R.S. Bubnova, M.G. Krzhizhanovskaya, I.G. Polyakova, S.K. Filatov, In situ high-temperature X-ray diffraction study of the Rb_2O-B_2O_3 glass forming system, Cryst. Res. Technol. 40 (2005) 73–82.
[33] N.A. Xie, Y.L. Huang, X.B. Qiao, L. Shi, H.J. Seo, A red-emitting phosphor of fully concentrated Eu^{3+}-based molybdenum borate $Eu_2MoB_2O_9$, Mater. Lett. 64 (2010) 1000–1002.
[34] F. Zhang, F.J. Zhao, K. Huang, X.P. Li, D.X. Han, X. Wang, H.M. Yin, High-resolution laser induced excitation spectroscopy and decay dynamics of $YNbO_4$:Er^{3+}, Spectrochim. Acta A. 267 (2022), 120573.
[35] K. Huang, F. Zhang, F.J. Zhao, H.M. Yin, Excited state trap in erbium doped borate glass, Chin. J. Chem. Phys. 35 (2022) 369–374.
[36] J.H. Dai, J.H. Lee, S.C. Lee, Annealing effect on the formation of In(Ga)AS quantum rings from InAs quantum dots, IEEE Photon. Technol. Lett. 20 (2008) 165–167.
[37] H.Y. Tai, Y.H. Lin, G.R. Lin, Wavelength-shifted yellow electroluminescence of Si quantum-dot embedded 20-Pair SiNx/SiOx superlattice by Ostwald Ripening Effect, IEEE Photon. J. 5 (2013), 6600110.
[38] R.S. Silva, F. Qu, A.M. Alcalde, N.O. Dantas, Atomic force microscopy and optical characterization of PbS quantum dots grown in glass matrix, Microelectron. J. 34 (2003) 647–649.
[39] A.A. de Thomaz, D.B. Almeida, V.B. Pelegati, H.F. Carvalho, S.G.C. Moreira, L.C. Barbosa, C.L. Cesar, The role of stress in CdTe quantum dot doped glasses, J. Phys. D Appl. Phys. 49 (2016) 1–5.
[40] Y.S. Zhu, G.C. Pan, L. Shao, G. Yang, X.M. Xu, J. Zhao, Y.L. Mao, Effective infrared emission of erbium ions doped inorganic lead halide perovskite quantum dots by sensitization of ytterbium ions, J. Alloys Compd. 835 (2020), 155390.
[41] X.T. Zhang, Y. Zhang, X.Y. Zhang, W.X. Yin, Y. Wang, H. Wang, M. Lu, Z.Y. Li, Z.Y. Gu, W.W. Yu, Yb^{3+} and Yb^{3+}/Er^{3+} doping for near-infrared emission and improved stability of $CsPbCl_3$ nanocrystals, J. Mater. Chem. C 6 (2018) 10101–10105.